GEOLOGY

Reevaluating the evidence for a Hadean-Eoarchean dynamo

Cauê S. Borlina[1]*, Benjamin P. Weiss[1], Eduardo A. Lima[1], Fengzai Tang[2], Richard J. M. Taylor[2], Joshua F. Einsle[2,3,4], Richard J. Harrison[2], Roger R. Fu[5], Elizabeth A. Bell[6], Ellen W. Alexander[6], Heather M. Kirkpatrick[6], Matthew M. Wielicki[7], T. Mark Harrison[6], Jahandar Ramezani[1], Adam C. Maloof[8]

Copyright © 2020 The Authors, some rights reserved; exclusive licensee American Association for the Advancement of Science. No claim to original U.S. Government Works. Distributed under a Creative Commons Attribution NonCommercial License 4.0 (CC BY-NC).

The time of origin of the geodynamo has important implications for the thermal evolution of the planetary interior and the habitability of early Earth. It has been proposed that detrital zircon grains from Jack Hills, Western Australia, provide evidence for an active geodynamo as early as 4.2 billion years (Ga) ago. However, our combined paleomagnetic, geochemical, and mineralogical studies on Jack Hills zircons indicate that most have poor magnetic recording properties and secondary magnetization carriers that postdate the formation of the zircons. Therefore, the existence of the geodynamo before 3.5 Ga ago remains unknown.

INTRODUCTION

Determining the history of the geodynamo before 3.5 Ga ago is limited by the lack of a well-preserved Archean-Hadean rock record. However, the discovery of Hadean detrital zircon grains in metasediments of the Jack Hills, Western Australia (*1*), opens up the possibility of studying the magnetic history of Earth during its first billion years. In particular, primary ferromagnetic inclusions (e.g., magnetite) in the zircons may contain a thermoremanent magnetization (TRM) that records the paleointensity of the ancient field during primary cooling (*2*–*5*).

To preserve such a record, magnetite-bearing zircon crystals must have avoided being heated above magnetite's 580°C Curie temperature over their subsequent histories (*3*, *6*). Furthermore, obtaining accurate paleointensity studies with well-determined ages for bulk zircon grains requires that the grains' natural remanent magnetization (NRM) be dominated by a TRM rather than a secondary crystallization remanent magnetization (CRM) carried by ferromagnetic inclusions formed or altered during aqueous alteration events after zircon crystallization (*3*, *6*).

Two recent studies (*7*, *8*) using single-crystal paleointensity analyses of Jack Hills zircon grains suggested that a geodynamo existed as early as 4.2 Ga ago with a surface field ~0.1 to 1 times that of present-day Earth. However, those studies (*7*, *8*) had three main limitations: (i) The ages of the NRMs in the grains analyzed are unknown (*3*, *9*); (ii) the grains were not shown to contain a TRM rather than a secondary CRM (*6*, *10*, *11*); (iii) the studies' grain selection criteria, which targeted grains with NRM intensities $>10^{-12}$ Am^2, might inadvertently have excluded zircons that would have recorded the absence of a dynamo (i.e., that carry no magnetization). In addition, there have been no independent studies corroborating their paleomagnetic measurements. The latter issue is particularly important because Jack Hills zircons have some of the weakest magnetic NRMs measured in the history of paleomagnetism and therefore require exceptionally sensitive magnetometry techniques and stringent contamination controls. To further evaluate the evidence of an early dynamo and address these limitations, we conducted coupled paleomagnetic, geochemical, and mineralogical analyses on Jack Hills detrital zircon grains.

We extracted the zircon crystals from the pebble conglomerate that we sampled in 2012 at the Hadean zircon discovery locality at Erawandoo Hill [site W74 (*3*, *9*)] using nonmagnetic techniques (see Materials and Methods). From these samples, 3754 zircons were washed with HCl acid and mounted in nonmagnetic epoxy, polished to approximately their midplanes, and dated using U-Pb chronometry. Grains found to have U-Pb ages older than 3.5 Ga (a total of 250) were analyzed using backscattered scanning electron (BSE) microscopy, cathodoluminescence (CL) imaging, and Li-ion imaging. BSE and CL images were used to assess the likelihood of secondary CRM by identifying zircon overgrowths, recrystallization zones, metamictization, cracks, and secondary deposits of minerals in void spaces (*12*). The goal of Li-ion imaging was to constrain the possibility of secondary TRM by providing estimates of the peak metamorphic temperatures experienced by zircons (*11*).

We defined a set of selection criteria that enables the identification of detrital zircon grains minimally affected by secondary TRM and CRM overprints (Fig. 1): (1) U-Pb age discordance <10% (see Materials and Methods); (2) lack of visible cracks, metamictization, and secondary deposits in BSE images and the presence of zonation in CL images interpreted as a primary igneous texture; and (3) presence of detectable primary Li zoning with thickness of <20 μm as observed by Li-ion imaging (*11*). Criterion (3) indicates the absence of TRM overprints acquired during ≳1 million years (Ma) long, ≳550°C metamorphic events under the assumption that natural Li diffusivity is similar to experimentally determined values (*13*). Note that these three criteria are based on measurements that only probe the polished surface of the grain (i.e., do not survey the full grain volume). Furthermore, the analytical methods used for criterion (2) are unable to resolve the <1-μm-diameter single-domain magnetite grains that would carry stable primary magnetization. Thus, these criteria likely are necessary but not sufficient requirements for identifying a zircon with primary NRM.

Of a total of 250 zircon grains, only 3 grains passed all of the above selection criteria. We selected these 3 grains, along with 53 grains

[1]Department of Earth, Atmospheric and Planetary Sciences, Massachusetts Institute of Technology (MIT), Cambridge, MA, USA. [2]Department of Earth Sciences, University of Cambridge, Cambridge, UK. [3]Department of Materials Science and Metallurgy, University of Cambridge, Cambridge, UK. [4]Department of Earth Science and Engineering, Imperial College London, London, UK. [5]Department of Earth and Planetary Sciences, Harvard University, Cambridge, MA, USA. [6]Department of Earth, Planetary, and Space Sciences, University of California, Los Angeles, Los Angeles, CA, USA. [7]Department of Geological Sciences, University of Alabama, Tuscaloosa, AL, USA. [8]Department of Geosciences, Princeton University, Princeton, NJ, USA.
*Corresponding author. Email: caue@mit.edu

Downloaded from http://advances.sciencemag.org/ on April 9, 2020

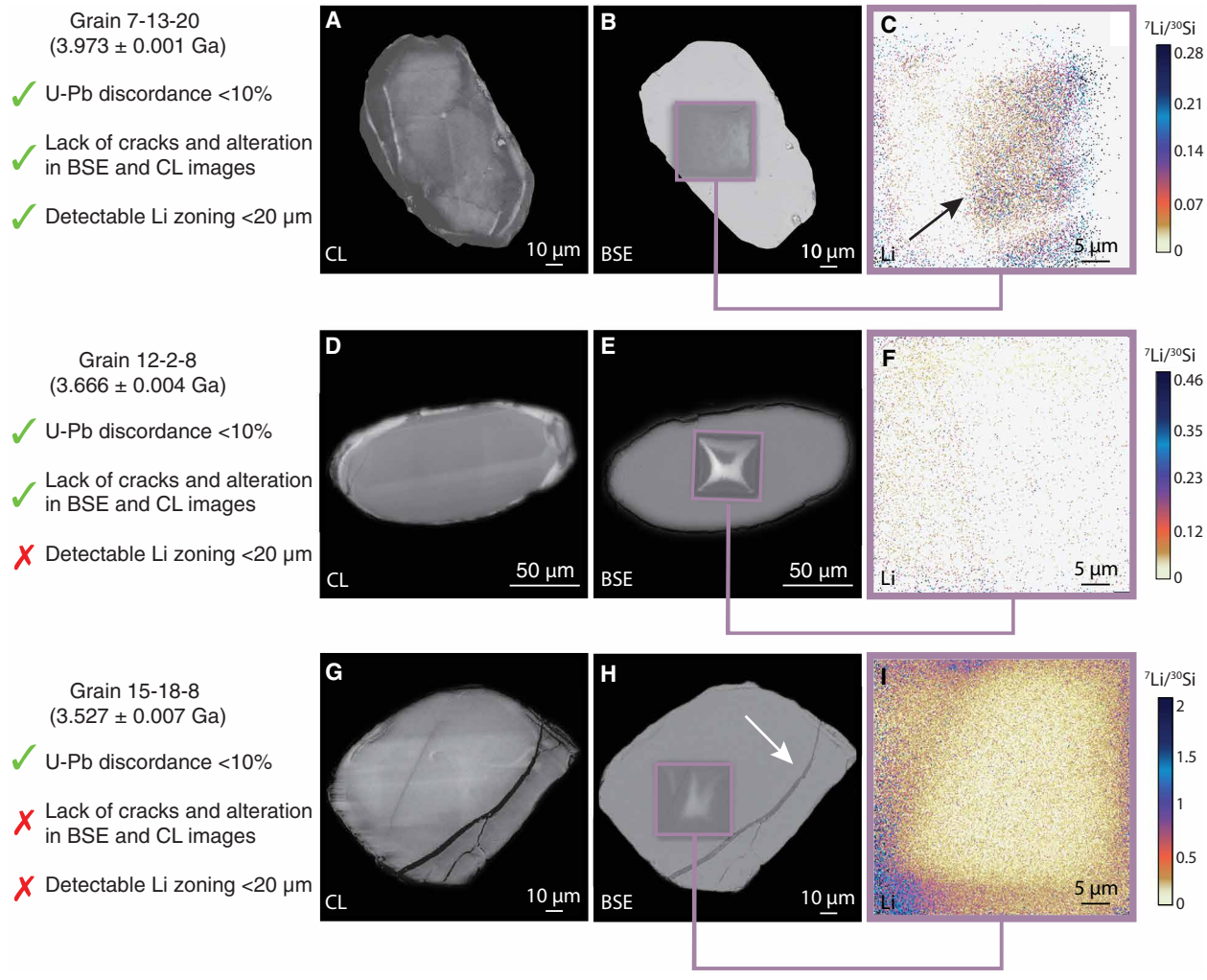

Fig. 1. Examples of grains that pass and fail the selection criteria. (**A** to **C**) Example of a zircon grain (7-13-20; 3.973 ± 0.001 Ga) that passes all selection criteria: U-Pb age discordance <10%, presence of zonation in CL (A), no signs of secondary deposits on the exposed surface from BSE (B), and <20-μm-thick Li zonation banding (black arrow), indicating that the sample may not have been fully thermally remagnetized since crystallization (C). (**D** to **F**) Example of a zircon grain (12-2-8; 3.666 ± 0.004 Ga) that passes some of the selection criteria: U-Pb age discordance <10%, presence of zonation in CL (D), no signs of secondary deposits on the exposed surface from BSE (E), and no observed Li zonation (F). (**G** to **I**) Example of a zircon grain (15-18-8; 3.527 ± 0.007 Ga) that fails most of the selection criteria: U-Pb age discordance <10%, absence of igneous zonation (G), presence of secondary mineral filling cracks at the lower right side of the grain (white arrow) (H), and no observed Li zonation (I).

that failed one or more criteria (including 13 subsamples from 6 grains; see Materials and Methods), for subsequent paleomagnetic studies. As a control to confirm that our polishing and ion and electron microprobe measurements do not fundamentally alter the zircons' NRMs, we also analyzed an additional 21 grains in their natural unpolished forms from the same host rocks using nonmagnetic methods, 4 of which were acid-washed. We conducted paleomagnetic analyses on a total of 77 grains.

Given the weak NRMs of the zircons (ranging between 6.05×10^{-15} and 4.15×10^{-12} Am^2 before demagnetization), their magnetic moments were analyzed using superconducting quantum interference device (SQUID) microscopy (see Materials and Methods) (*14*, *15*). Following methods previously developed for the Bishop Tuff zircons (*2*), we obtained paleointensity estimates for the 77 grains using the in-field zero-field zero-field in-field (IZZI) double-heating protocol (*16*) with partial TRM (pTRM) alteration checks at every other heating step starting at 300°C.

We defined paleomagnetic quality criteria that are permissive compared with those of typical paleointensity studies of younger rocks (see the Supplementary Materials). This is because the overall goal of this study was to establish the presence or absence of a geodynamo at >3.5 Ga ago, which only requires paleointensities with order-of-magnitude uncertainties. Therefore, paleointensity estimates were considered acceptable when a sample (a) had a difference ratio sum ≤25% (*17*) and (b) gained a moment in the direction of the laboratory field during in-field steps with a maximum angular deviation ≤15° (*18*). Criterion (a) indicates that minimal thermochemical alteration occurred during the paleointensity experiments, while criterion (b) provides evidence that the sample can record an ancient field's direction and intensity (while not requiring the presence or absence of such a field when the zircon acquired its magnetic record). In summary, samples that pass our initial selection criteria and paleomagnetic criteria are candidates for providing a robust constraint on the dynamo at the time of their crystallization. Conversely, samples

Downloaded from http://advances.sciencemag.org/ on April 9, 2020

with unstable NRM would either indicate the absence of a dynamo (if the sample passes the selection and paleomagnetic criteria) or that the sample is unsuitable for paleointensity experiments (either because of poor magnetic recording properties and/or sample alteration during laboratory heating). Following the paleointensity experiments, we analyzed selected grains with quantum diamond magnetometry (QDM) (*19*) coupled with transmission electron microscopy (TEM) to elucidate the origin of the magnetic sources within the grains.

RESULTS

Of the 77 zircon grains analyzed for paleointensity estimations, only a total of 6 grains passed the two paleomagnetic criteria. We found that 63 of the 77 samples failed paleomagnetic criterion (a), indicating alteration during our experiments. In addition, we found that 54 samples have poor magnetic recording properties, as indicated by their failure of paleomagnetic criterion (b). Among the six grains that passed both paleomagnetic criteria, only two passed all five combined selection and paleomagnetic criteria (Fig. 2). Even if we were to exclude Li zonation as one of the selection criteria, there would be no additional grains that would pass the other selection and paleomagnetic criteria (*13*). In addition, our analyses of the unpolished control grains confirm that polishing the grains did not increase the incidence of alteration during experiments or the magnetic recording quality (see the Supplementary Materials).

The two grains that passed the five combined criteria were sample 7-13-20, with a U-Pb age of 3.973 ± 0.001 Ga, and sample 8-2-11, with a U-Pb age of 3.979 ± 0.007 Ga. Figure 2 summarizes the selection process starting from the initial 3754 grains and ending at these 2 grains. Figures 3 and 4 show BSE, CL, Li, and paleomagnetic data for these two grains. The two grains each have at least two NRM components. Sample 7-13-20 (Fig. 3) has a low-temperature component that unblocked between room temperature and 200°C, a medium-temperature component that unblocked between 200° and 300°C, and a high-temperature component that unblocked between 300° and 580°C. Sample 8-2-11 (Fig. 4) has a low-temperature component that unblocked between room temperature and 510°C and a high temperature component that unblocked between 510° and 580°C. The 580°C peak demagnetization temperature of the NRMs for both samples indicates that the high-temperature components are carried by nearly pure magnetite.

Figure 5 shows an example of a grain that passes all of the selection criteria but fails all of the paleomagnetic criteria. Most of our grains present NRM demagnetization similar to the one in Fig. 5: unstable demagnetization, thermochemical alteration in the laboratory, and no in-field acquisition of remanence.

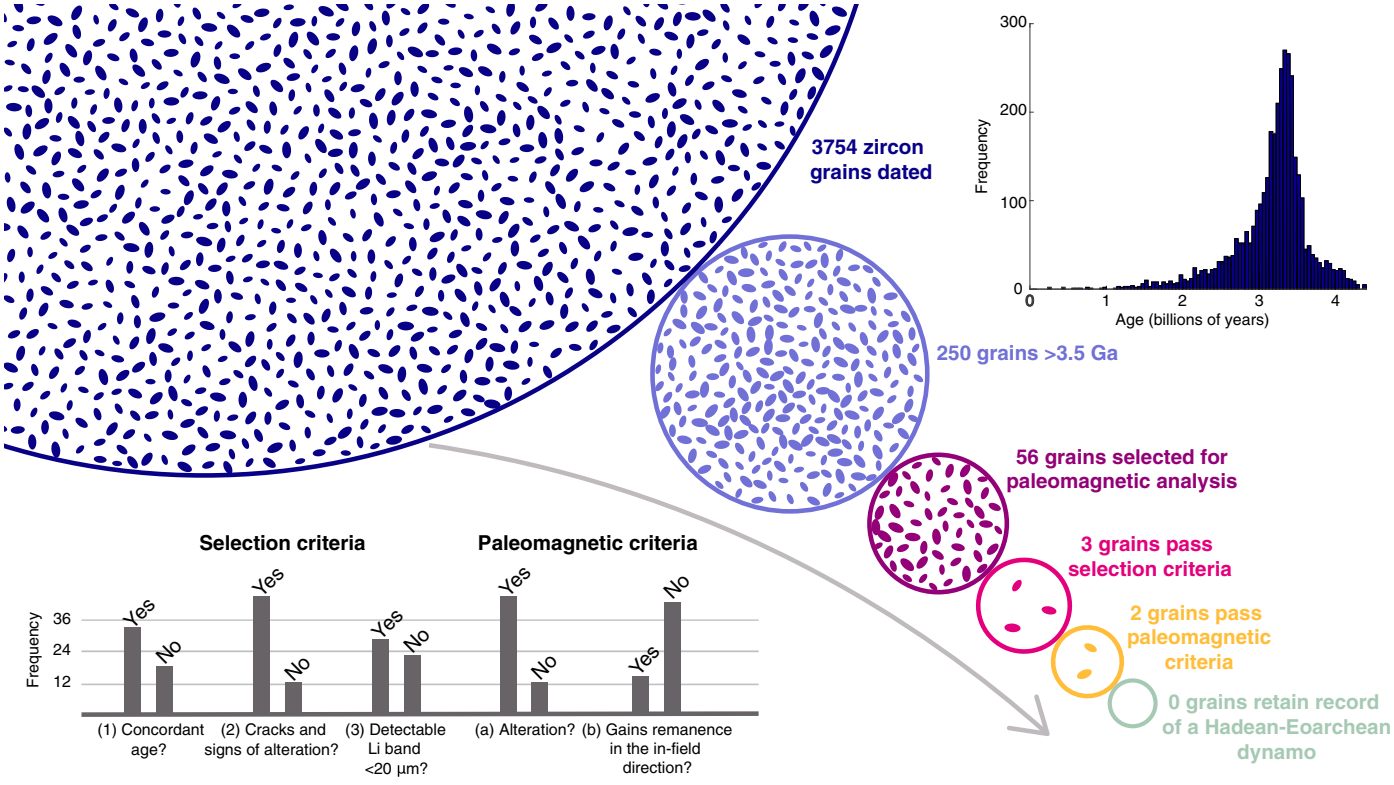

Fig. 2. Summary of zircon selection from the initial 3754 dated grains. Each circle shows the number of zircon grains remaining after each selection step. The histogram on the top right shows the measured age distribution of the 3754 grains. From the 250 grains that were older than 3.5 Ga, we selected all grains that passed all the selection criteria (3 grains) and an additional set of 53 grains. The histograms at the bottom left show the number of grains that satisfy the various selection criteria [(1) U-Pb age discordance <10%; (2) lack of visible cracks, metamictization, and secondary deposits; and (3) detectable primary Li zoning with thickness of <20 µm] and paleomagnetic criteria [(a) the NRM component had a difference ratio sum ≤25%, and (b) the sample gained a moment in the direction of the laboratory field during in-field steps with a maximum angular deviation ≤15° over the same temperature range as the NRM component] for the 56 grains selected for paleomagnetic analysis. Only two grains pass all the selection and paleomagnetic criteria. In addition to the 56 polished grains shown here, 21 whole grains were also analyzed paleomagnetically as a control. No grain showed evidence for a Hadean-Eoarchean dynamo.

Downloaded from http://advances.sciencemag.org/ on April 9, 2020

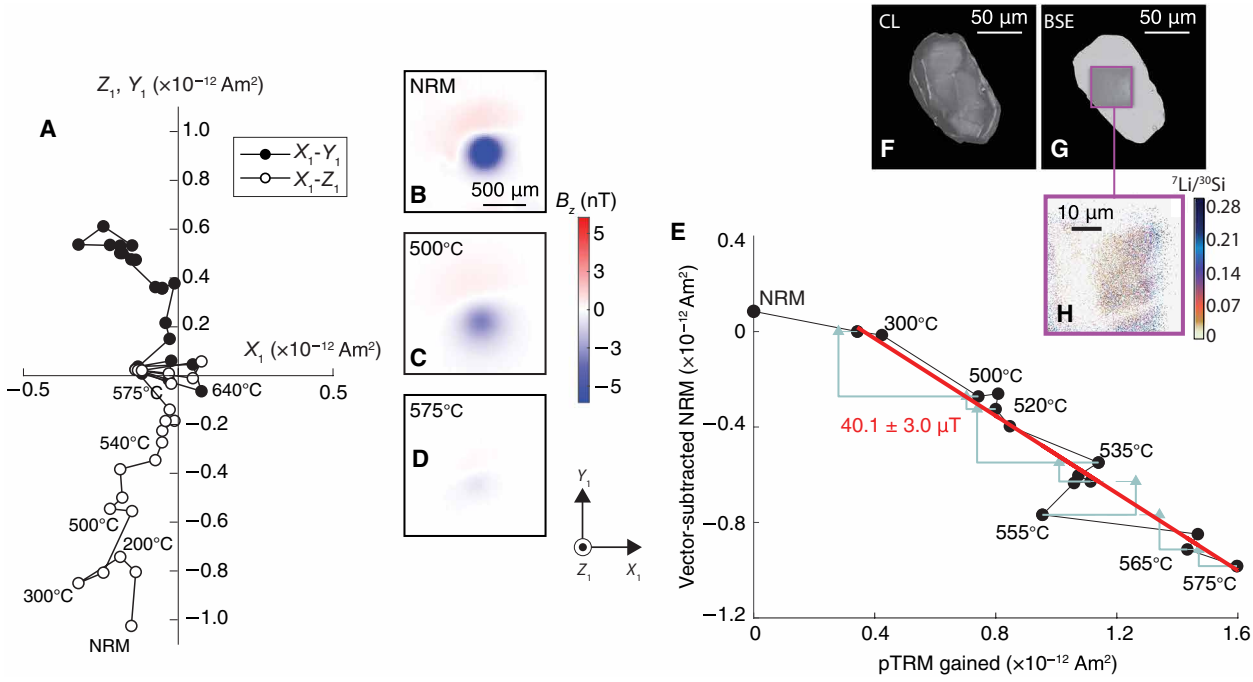

Fig. 3. Paleomagnetic data for zircon grain 7-13-20 (3.973 ± 0.001 Ga) that passes all selection and paleomagnetic criteria. (**A**) Orthographic projection of NRM vector endpoints during thermal demagnetization. Closed symbols show the *X*-*Y* projection of the magnetization; open symbols show *Z*-*Y* projection of the magnetization. Selected demagnetization steps are labeled. (**B** to **D**) Out-of-the-page magnetic field component (B_z) maps measured at a height of ~360 μm above the grains obtained with the SQUID microscope for the NRM, 500°C, and 575°C steps. We use a "1" subscript on X_1, Y_1, and Z_1 to denote the fact that the grain orientations during the thermal demagnetization and paleointensity experiments are different from the grain orientations during the BSE, CL, and Li measurements and during the QDM measurements (Fig. 6). (**E**) Vector-subtracted NRM from the 300°C step versus pTRM grained during progressive laboratory heating. Blue triangles show pTRM checks. The red line shows the measurements used to compute paleointensity values (300° to 580°C). (**F** to **H**) CL, BSE, and Li images of the grains.

Subsequent to the paleointensity studies, grains 7-13-20 and 8-2-11 were analyzed in more detail to elucidate the nature and origin of their ferromagnetic inclusions. First, the isothermal remanent magnetization (IRM) of the samples was imaged with QDM (*19*) to determine the location of the magnetization sources (Fig. 6). Following this, we used TEM to investigate internal regions with the strongest magnetization. We found no evidence of primary ferromagnetic inclusions. Instead, we observed magnetite crystals (identified using Moiré diffraction interferometry) (*10*) growing inside voids fed by iron that diffused along the regions of intersecting dislocations. We also identified magnetite crystals with high aspect ratios, crystallographically aligned with the host zircon, and growing along dislocation cores [Fig. 6; see also (*10*)]. The alignment, aspect ratios, and locations of the magnetite grains within regions of recovery from accumulated radiation damage demonstrate that the grains are secondary in origin (*20*–*22*). No evidence has been put forth to support the speculation that they formed by exsolution and/or vapor deposition (*8*). The presence of secondary magnetite is not linked to alteration during laboratory heating steps, as demonstrated by the fact that these two grains passed paleomagnetic criterion (a) and that they contain voids with a diversity of shapes and sizes that commonly are empty or filled with phases other than magnetite, most commonly baddeleyite and ilmenite (*23*). The magnetite apparently formed as a result of natural fluid alteration at an unknown time during the last 3.9 Ga, at which time their bulk host zircons would have acquired a secondary CRM.

DISCUSSION

The data presented here suggest that the vast majority of Jack Hills zircons are not suitable for paleointensity studies of the Hadean-Eoarchean magnetic field. In particular, only 2 of 77 grains passed our five selection and paleomagnetic criteria. These two grains yielded results similar to those previously reported for Jack Hills zircons (*7*, *8*) and that were interpreted to be a record of a Hadean-Eoarchean dynamo: initial NRM intensities of ~1×10^{-12} Am^2, no signs of alteration, and stable NRM demagnetization exhibiting multiple components. However, close examination of both of our grains shows that their magnetic carriers are most likely secondary in origin. Therefore, the ages of their NRMs are unknown and certainly younger than their U-Pb ages. Their multicomponent NRMs are consistent with being CRMs overprinted by pTRMs because of heating events in the Jack Hills outcrop or else by younger CRMs. The presence of a CRM means that the thermal paleointensity experiments, which implicitly assume that the NRM is a TRM, will yield unreliable paleointensity values. We also note that unlike the previous studies (*7*, *8*), we found that the majority of grains analyzed paleomagnetically have poor demagnetization and remagnetization behavior. In conclusion, the existence of the dynamo before 3.5 Ga has yet to be established.

We suggest that the difference in results between our study and that of (*7*, *8*) may be due to our different measurement protocol, in which we washed the grains using concentrated (6 M) HCl to remove considerable amounts of secondary magnetic deposits before paleomagnetic

Downloaded from http://advances.sciencemag.org/ on April 9, 2020

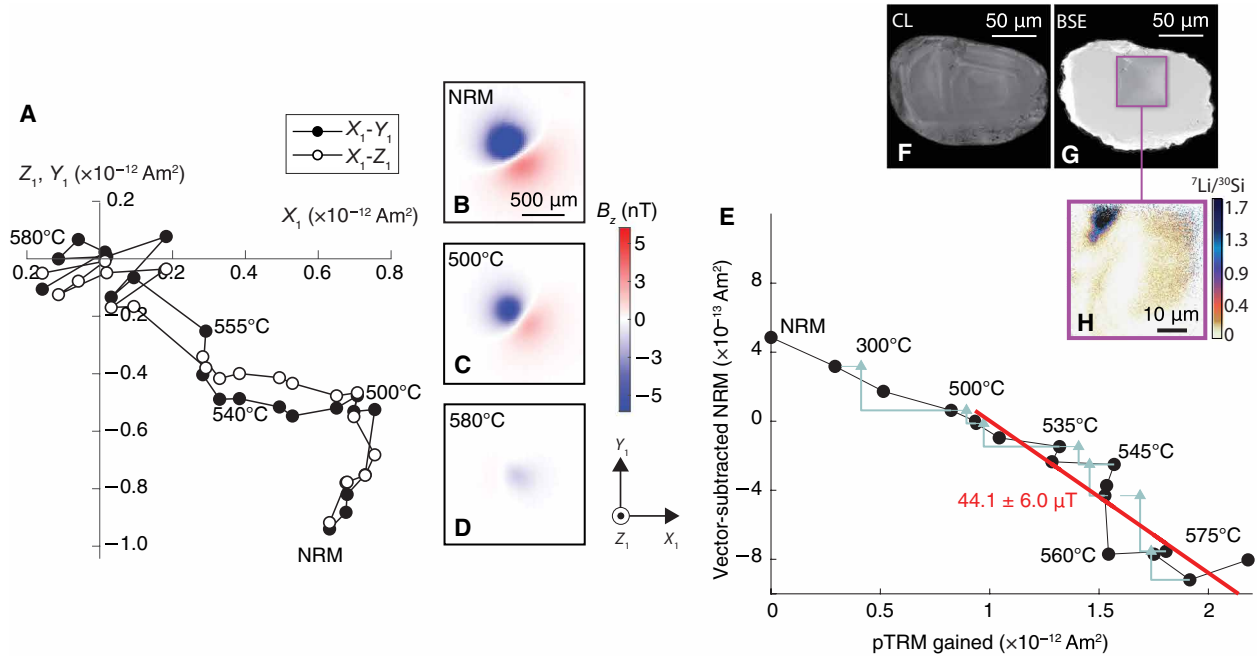

Fig. 4. Paleomagnetic data for zircon grain 8-2-11 (3.979 ± 0.007 Ga) that passes all selection and paleomagnetic criteria. (**A**) Orthographic projection of NRM vector endpoints during thermal demagnetization. Closed symbols show *X-Y* projection of the magnetization; open symbols show *Z-Y* projection of the magnetization. Selected demagnetization steps are labeled. (**B** to **D**) Out-of-the-page magnetic field component (B_z) maps measured at a height of ~360 µm above the grains obtained with the SQUID microscope for the NRM, 500°C, and 575°C steps. We use a "1" subscript on X_1, Y_1, and Z_1 to denote the fact that the grain orientations during the thermal demagnetization and paleointensity experiments are different from those during the BSE, CL, and Li measurements and during the QDM measurements (Fig. 6). (**E**) Vector-subtracted NRM from the 510°C step versus pTRM grained during progressive laboratory heating. Blue triangles show pTRM checks. The red line shows the measurements used to compute paleointensity values (510° to 580°C). (**F** to **H**) CL, BSE, and Li images of the grains.

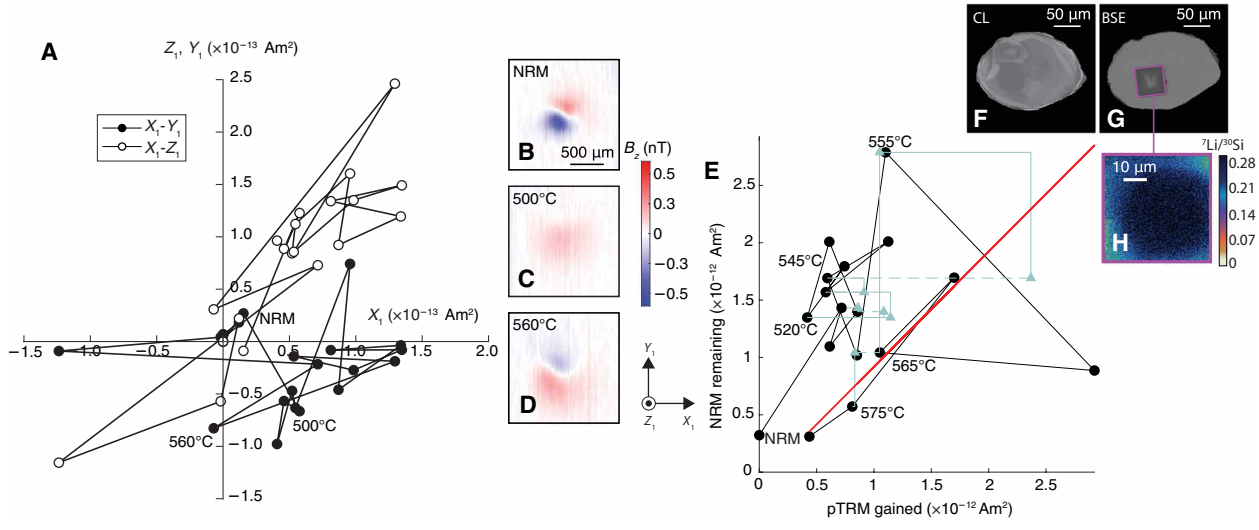

Fig. 5. Paleomagnetic data for zircon grain 15-1-7 (4.094 ± 0.005 Ga) that passes the selection criteria but fails the paleomagnetic criteria. (**A**) Orthographic projection of NRM vector endpoints during thermal demagnetization. Closed symbols show *X-Y* projection of the magnetization; open symbols show *Z-Y* projection of the magnetization. Selected demagnetization steps are labeled. (**B** to **D**) Out-of-the-page magnetic field component (B_z) maps at a height of ~360 µm above the grains obtained with the SQUID microscope for the NRM, 500°C and 580°C steps. We use a "1" subscript on X_1, Y_1 and Z_1 to denote the fact that the grain orientations during the thermal demagnetization and paleointensity experiments are different from the grain orientations during the BSE, CL, and Li measurements. (**E**) NRM lost versus pTRM grained during progressive laboratory heating. Blue triangles show pTRM checks. Red line shows the measurements used to compute paleointensity values (550° to 580°C). (**F** to **H**) CL, BSE, and Li images of the grains.

Downloaded from http://advances.sciencemag.org/ on April 9, 2020

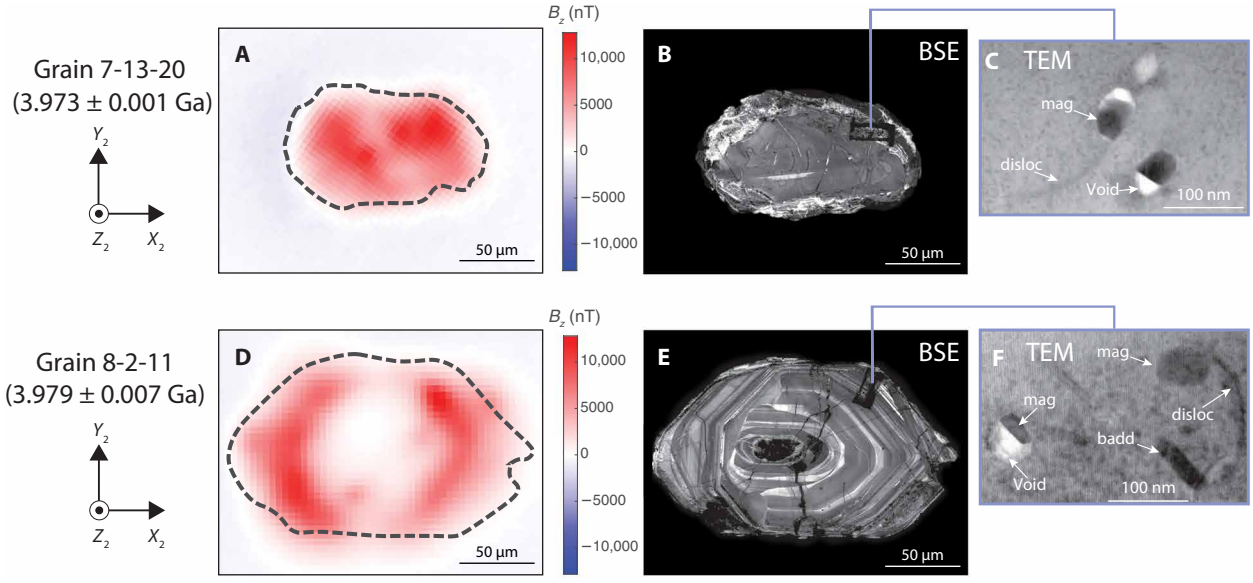

Fig. 6. Magnetite grains located in dislocations and filling parts of voids postdating igneous formation of the zircon host. (**A** to **C**) Zircon grain 7-13-20. (**D** to **F**) Zircon grain 8-2-11. (A and D) QDM maps of the out-of-the-page magnetic field component (B_z) of an IRM applied to the grain used to locate magnetic sources at a height of ~5 μm above the samples. We use X_2, Y_2, and Z_2 to denote that the grain orientations for these measurements differ from those during the paleointensity experiments (Figs. 3 to 5). (B and E) BSE images of the grains. The grains were repolished after the paleomagnetic experiments and before these BSE images. Note the difference when compared with the earlier BSE images of the same grains in Figs. 3 and 4; the images here expose several cracks that were not previously visible. (C and F) TEM analyses conducted in the vicinity of the strongest magnetic region of the grain by extracting rectangular focused ion beam sections (from rectangular regions visible in the BSE images). Magnetite ("mag") grains are seen to be forming inside voids that intersect dislocations ("disloc") and growing along dislocation cores that formed during recovery. Magnetite commonly is associated with baddeleyite ("badd"), a secondary product formed after recovery from radiation damage (*23*), pointing to the fact that the magnetite crystals were not present in the zircon structure when the zircon crystal formed.

measurements, used high-sensitivity magnetic microscopy that enabled measurements of samples with up to 1000 times weaker NRMs, and used QDM and TEM to constrain whether the magnetic carriers are primary in origin. Elucidating the early evolution of the geodynamo may require as yet unidentified detrital minerals that are less prone to radiation damage.

MATERIALS AND METHODS

Source location of the samples

Our field work was conducted in the Jack Hills in 2002 and 2012. We separated zircons from five rock samples (named D175C, D175H, D175L, and Cong14c) collected at the Hadean zircon discovery site, location W74 (*24*), in the Jack Hills, Western Australia, Australia (*1*), during the 2012 field trip. Table S1 shows the sampling information about the bulk samples and the source material for the grains.

Zircon separation from host rocks

The five rock samples were manually sledged to gravel size fragments in the Massachusetts Institute of Technology (MIT) Isotope Laboratory. These fragments then were pulverized in a Shatterbox using an all-ceramic grinding vessel and sieved to <500-μm grain size. The material then was mixed in water in a 4-liter beaker, and the suspended material (<~5 μm) was decanted; this wash process was repeated 15 times. The remaining sand- and silt-size fraction then was dried under a heat lamp (maximum temperature of 45°C). The heavy-mineral aliquot was separated by immersion in a high-density liquid (methylene iodide; specific gravity, 3.32), followed by rinsing in acetone and air drying. Zircon grains then were handpicked under a binocular microscope using nonmagnetic tweezers. Note that our separation procedures did not involve the standard use of a Frantz isodynamic separator for removing paramagnetic and ferromagnetic minerals, as the high magnetic field of the Frantz would otherwise alter any original NRM that might have been present in the grains.

Ion and electron microprobe measurements

U and Pb isotopes, backscattered electron microscopy (BSE microscopy), CL, and Li-ion measurements were carried out in the UCLA Secondary Ion Mass Spectrometry (SIMS) Laboratory at the University of California, Los Angeles (UCLA). The samples were transported between MIT and UCLA in magnetically shielded cans. Approximately 400 grains were placed in 10 separate 2.5-cm-diameter epoxy EPO-TEK 301 mounts and polished to approximately their midplanes. Information about bulk rock source for the zircon grains and their respective mount number are compiled in table S1. U and Pb isotopes were measured on a CAMECA IMS 1270 SIMS, using an $^{16}O^-$ primary beam, with beam currents of 12 to 15 nA. A beam diameter of ~20 to 30 μm was used. Isotopes measured were $^{94}Zr^2O$, ^{204}Pb, ^{206}Pb, ^{207}Pb, ^{208}Pb, ^{232}Th, ^{238}U, and $^{238}U^{16}O$. The mass-resolving power was ≥5500. We used oxygen flooding for improved Pb ionization (*25*). For the common Pb correction, we used a ^{204}Pb correction assuming laboratory contamination with environmental Pb from southern California, specifically the San Diego sewage (*26*), with common $^{206}Pb/^{204}Pb$ = 18.86, common $^{207}Pb/^{204}Pb$ = 15.62, and common $^{208}Pb/^{204}Pb$ = 38.34. An initial $^{206}Pb/^{207}Pb$ ratio survey on 3754 grains was used to identify grains older than 3.5 Ga for all mounts except UCLA 1, 2, and 3; the latter were instead surveyed for grains older than 3.8 Ga. U-Pb measurements and BSE, CL, and

Downloaded from http://advances.sciencemag.org/ on April 9, 2020

Li images were then acquired from grains that passed this criterion. We calculated the $^{207}Pb/^{206}Pb$ and $^{206}Pb/^{238}U$ dates and inferred the $^{207}Pb/^{235}U$ using the known U isotope ratio ($^{238}U/^{235}U = 137.88$). We assigned ages using $^{207}Pb/^{206}Pb$ ratios. $^{207}Pb/^{206}Pb$ and $^{206}Pb/^{238}U$ were used to compute the discordance (*27*, *28*)

$$\left| \frac{\frac{^{207}Pb}{^{206}Pb}}{\frac{^{206}Pb}{^{238}Pb}} - 1 \right| \times 100\% \quad (1)$$

Table S2 compiles U-Pb measurements for the grains that passed the initial $^{206}Pb/^{207}Pb$ survey. Table S3 contains age and uncertainties for the 77 grains selected for the paleomagnetic experiments. BSE and CL images were acquired with a TESCAN VEGA3 scanning electron microscope equipped with a TESCAN three-channel color CL detector and TESCAN retractable BSE detector (*29*).

Li-ion images were acquired using a CAMECA IMS 1290 SIMS at the UCLA SIMS Laboratory. We used the Hyperion II radio frequency plasma primary ion source (*30*) with a 250 to 300 pA $^{16}O^-$ beam focused to a <1-μm spot size. We rastered the beam over a 50 × 50–μm area and recorded 10 frames of ion images of ^7Li and ^{30}Si. We used the program WinImage to accumulate the 10 frames each of ^7Li and ^{30}Si (image intensity was integrated over all 10 frames), and computed the ratio of the two to get an image of $^7Li/^{30}Si$ intensity. We normalized ^7Li to ^{30}Si to account for charging (where the ionization rate may be heterogeneous because of accumulation of charge in the sample as it is continually bombarded with negative secondary ions). The spatial resolution of the images is equivalent to the spot size, so any feature >1 μm is not an artifact. Because boundaries on zones are resolved to ≤1 μm, blurring of zones by more than this value means they are actually physically smooth over that length scale. A detectable Li zoning with thickness of <20 μm provides evidence that the sample has not been heated >550°C for more than 1 million years (*11*). However, this method might provide an underestimation of the peak temperature experienced by the grains in some cases (*13*). As discussed in the main text, whether or not the Li band criterion is used to filter our samples does not change the overall outcome of this study. In the Supplementary Materials, we provide evidence that the ion and electron microprobe work measurements did not remagnetize the samples. We also provide the complete set of images taken from all measured grains.

Acid washing

We previously showed that most Jack Hills zircon grains, when untreated with concentrated (6 M) hydrochloric acid (HCl) acid, have magnetization likely dominated by secondary minerals coating the zircons (*6*). Therefore, before paleomagnetic measurements, all grains analyzed here (with the exception of four whole grains; see section S5 of the Supplementary Materials) were washed with a 6 M HCl solution for 12 min at room temperature, followed by rinsing in Milli-Q water and air drying. Zircon crystals from samples D175C and D175H were washed with HCl before U-Pb measurements, while grains from D175L and Cong14C were washed with HCl after U-Pb measurements. All grains selected for paleomagnetic measurements were extracted from the epoxy mounts using nonmagnetic tools (Semprex probe needle, lot 18) and washed in 70% sulfuric acid (H_2SO_4) for 3 hours to remove any residual epoxy deposits before magnetic measurements. During extraction, five samples (18-8-12, 18-15-18, 18-4-8, 1-1-9, and 18-2-12) fragmented into two pieces and one sample (18-11-13) fragmented into three pieces. All acid washing steps were performed in the MIT Isotope Laboratory cleanroom facilities.

Paleomagnetism

Following HCl and H_2SO_4 acid-washing, grains were mounted in pits drilled into Corning Eagle XG glass slides, following similar procedures previously developed for analyzing zircons from the Bishop Tuff (*2*). Figure S3 shows the overall measuring setup. Optical and magnetic field images of the four glass holders with the grains mounted in the pits before demagnetization are shown in fig. S4. The absolute orientation of the grains was not maintained between mounting in the epoxy for the electron microscopy and ion probe measurements and in the glass mount for paleomagnetic measurements. However, the orientation of the grains and the glass mount was kept fixed throughout the paleomagnetic measurements.

Heating steps were conducted with an ASC Scientific TD48-SC thermal demagnetizer, which provides temperature control with accuracy of better than ±5°C. An IZZI protocol was used in this experiment (*16*). The in-field step used a 50-μT laboratory magnetic field.

Because of the overall weak magnetic moments of the samples (between 6.05×10^{-15} and 4.15×10^{-12} Am^2), NRM measurements were conducted with the SQUID microscope (*14*) in the MIT Paleomagnetism Laboratory. The configuration used in these experiments, including the sample holder and the mount with the zircon crystals, yields an approximate distance from the SQUID sensor to the midplane of the sample of ~360 μm (fig. S3). This distance includes the sensor to the window separation (~200 μm), the thickness of the Corning Eagle XG glass left at the bottom of the wells (~60 μm), and half of the size of the grain (~100 μm).

Using SQUID microscopy, we mapped the out-of-the-plane component of the magnetic field of individual zircons at a fixed distance above the sample. Maps were 3 mm × 3 mm in size with spatial sampling of 25 μm. Magnetic field maps were subsequently inverted for the magnetic moment using previously validated techniques (*2*, *15*). At each demagnetization/remagnetization step, zircon grains with moments $<1 \times 10^{-13}$ Am^2 were measured four times and the inverted moments averaged to obtain accurate estimates of their net moments, while stronger magnetic samples were measured only once. When magnetic sources were not observed in our measurements, we assumed a maximum magnetic moment of $\sim 6 \times 10^{-15}$ Am^2, which is the noise floor of the MIT SQUID microscope at this sensor-sample distance. All magnetic measurements, including magnetic maps and processed data, are located in the dataset (see the Supplementary Materials) and will be uploaded to the Magnetics Information Consortium (MagIC) database.

Quantum diamond microscopy

After paleomagnetic measurements, select grains were extracted from the glass mount, placed in epoxy EPO-TEK 301, and polished again. We used the QDM (*19*) in the Harvard Paleomagnetics Laboratory to constrain the location of the magnetization carriers within the grains. Samples were measured in contact with the sensing diamond after a 0.4-T IRM was applied in the out-of-plane direction using an ASC model IM-10-3 impulse magnetizer. We measured the magnetic field intensity at a height of ~5 μm above the sample along the [111] direction of the diamond crystal lattice using projective magnetic microscopy with a resolution of 1.17 micrometers per

Downloaded from http://advances.sciencemag.org/ on April 9, 2020

pixel (*19*). We isolated the remanent field signal of ferromagnetic grains by measuring the sample successively under two mutually antiparallel 0.9-mT bias fields and computing the out-of-plane magnetic field using a spectral algorithm (*15*). Figure 6 shows the QDM measurements. The absolute orientation of the grains differed between the SQUID microscopy measurements and these QDM measurements.

Transmission electron microscopy

TEM was conducted in the Wolfson Electron Microscopy Suite at the University of Cambridge. Our TEM analysis targeted locations based on the QDM maps previously measured. The TEM foil was prepared using a dual-beam focused ion beam microscope FEI Helios NanoLab (Hillsboro, OR, USA) with an area of ~60 μm^2 and a depth of ~7 μm. An in-situ lift-out technique was used to site-specifically extract the foil from the place with magnetic signals mapped with the QDM, and a cleanup procedure with low acceleration voltage was used to reduce surface damage of the foil. The TEM sample was examined using a FEI Tecnai Osiris TEM with an extreme Schottky field emission gun. The instrument was equipped with four large-area energy-dispersive x-ray spectrometer detectors, providing a fast chemical compositional measurement. The analysis was carried out at scanning TEM mode at 200 kV, where both bright-field and high-angle annular dark-field images were acquired.

SUPPLEMENTARY MATERIALS

Supplementary material for this article is available at http://advances.sciencemag.org/cgi/content/full/6/15/eaav9634/DC1

REFERENCES AND NOTES

1. W. Compston, R. T. Pidgeon, Jack Hills, evidence of more very old detrital zircons in Western Australia. *Nature* **321**, 766–769 (1986).
2. R. R. Fu, B. P. Weiss, E. A. Lima, P. Kehayias, J. F. D. F. Araujo, D. R. Glenn, J. Gelb, J. F. Einsle, A. M. Bauer, R. J. Harrison, G. A. H. Ali, R. L. Walsworth, Evaluating the paleomagnetic potential of single zircon crystals using the Bishop Tuff. *Earth Planet. Sci. Lett.* **458**, 1–13 (2017).
3. B. P. Weiss, A. C. Maloof, N. Tailby, J. Ramezani, R. R. Fu, V. Hanus, D. Trail, E. Bruce Watson, T. M. Harrison, S. A. Bowring, J. L. Kirschvink, N. L. Swanson-Hysell, R. S. Coe, Pervasive remagnetization of detrital zircon host rocks in the Jack Hills, Western Australia and implications for records of the early geodynamo. *Earth Planet. Sci. Lett.* **430**, 115–128 (2015).
4. J. A. Tarduno, E. G. Blackman, E. E. Mamajek, Detecting the oldest geodynamo and attendant shielding from the solar wind: Implications for habitability. *Phys. Earth Planet. Inter.* **233**, 68–87 (2014).
5. M. Sato, S. Yamamoto, Y. Yamamoto, Y. Okada, M. Ohno, H. Tsunakawa, S. Maruyama, Rock-magnetic properties of single zircon crystals sampled from the Tanzawa tonalitic pluton, central Japan. *Earth Planets Space* **67**, 150 (2015).
6. B. P. Weiss, R. R. Fu, J. F. Einsle, D. R. Glenn, P. Kehayias, E. A. Bell, J. Gelb, J. F. D. F. Araujo, E. A. Lima, C. S. Borlina, P. Boehnke, D. N. Johnstone, T. M. Harrison, R. J. Harrison, R. L. Walsworth, Secondary magnetic inclusions in detrital zircons from the Jack Hills, Western Australia, and implications for the origin of the geodynamo. *Geology* **46**, 427–430 (2018).
7. J. A. Tarduno, R. D. Cottrell, W. J. Davis, F. Nimmo, R. K. Bono, A Hadean to Paleoarchean geodynamo recorded by single zircon crystals. *Science* **349**, 521–524 (2015).
8. J. A. Tarduno, R. D. Cottrell, R. K. Bono, H. Oda, W. J. Davis, M. Fayek, O. van 't Erve, F. Nimmo, W. Huang, E. R. Thern, S. Fearn, G. Mitra, A. V. Smirnov, E. G. Blackman, Paleomagnetism indicates that primary magnetite in zircon records a strong Hadean geodynamo. *Proc. Natl. Acad. Sci.* **117**, 2309–2318 (2020).
9. B. P. Weiss, A. C. Maloof, T. M. Harrison, N. L. Swanson-Hysell, R. R. Fu, J. L. Kirschvink, E. Bruce Watson, R. S. Coe, S. M. Tikoo, J. Ramezani, Reply to comment on "Pervasive remagnetization of detrital zircon host rocks in the Jack Hills, Western Australia and implications for records of the early dynamo". *Earth Planet. Sci. Lett.* **450**, 409–412 (2016).
10. F. Tang, R. J. M. Taylor, J. F. Einsle, C. S. Borlina, R. R. Fu, B. P. Weiss, H. M. Williams, W. Williams, L. Nagy, P. A. Midgley, E. A. Lima, E. A. Bell, T. M. Harrison, E. W. Alexander, R. J. Harrison, Secondary magnetite in ancient zircon precludes analysis of a Hadean geodynamo. *Proc. Natl. Acad. Sci. U.S.A.* **116**, 407–412 (2018).
11. D. Trail, D. J. Cherniak, E. B. Watson, T. M. Harrison, B. P. Weiss, I. Szumila, Li zoning in zircon as a potential geospeedometer and peak temperature indicator. *Contrib. Mineral. Petrol.* **171**, 1–15 (2016).
12. F. Corfu, J. M. Hanchar, P. W. O. Hoskin, P. Kinny, Atlas of zircon textures. *Rev. Mineral. Geochemistry* **53**, 469–500 (2003).
13. M. Tang, R. L. Rudnick, W. F. McDonough, M. Bose, Y. Goreva, Multi-mode Li diffusion in natural zircons: Evidence for diffusion in the presence of step-function concentration boundaries. *Earth Planet. Sci. Lett.* **474**, 110–119 (2017).
14. B. P. Weiss, E. A. Lima, L. E. Fong, F. J. Baudenbacher, Paleomagnetic analysis using SQUID microscopy. *J. Geophys. Res.* **112**, 1–20 (2007).
15. E. A. Lima, B. P. Weiss, Ultra-high sensitivity moment magnetometry of geological samples using magnetic microscopy. *Geochem. Geophys. Geosyst.* **17**, 3754–3774 (2016).
16. Y. Yu, L. Tauxe, A. Genevey, Toward an optimal geomagnetic field intensity determination technique. *Geochem. Geophys. Geosyst.* **5**, Q02H07 (2004).
17. L. Tauxe, H. Staudigel, Strength of the geomagnetic field in the cretaceous normal superchron: New data from submarine basaltic glass of the Troodos Ophiolite. *Geochem. Geophys. Geosyst.* **5**, Q02H06 (2004).
18. J. L. Kirschvink, The least-squares line and plane and the analysis of paleomagnetic data. *Geophys. J. Roy. Astron. Soc.* **62**, 699–718 (1980).
19. D. R. Glenn, R. R. Fu, P. Kehayias, D. Le Sage, E. A. Lima, B. P. Weiss, R. L. Walsworth, Micrometer-scale magnetic imaging of geological samples using a quantum diamond microscope. *Geochem. Geophys. Geosyst.* **18**, 3254–3267 (2017).
20. L. F. White, J. R. Darling, D. E. Moser, D. A. Reinhard, T. J. Prosa, D. Bullen, D. Olson, D. J. Larson, D. Lawrence, I. Martin, Atomic-scale age resolution of planetary events. *Nat. Commun.* **8**, 15597 (2017).
21. N. E. Timms, S. M. Reddy, J. D. Fitz Gerald, L. Green, J. R. Muhling, Inclusion-localised crystal-plasticity, dynamic porosity, and fast-diffusion pathway generation in zircon. *J. Struct. Geol.* **35**, 78–89 (2012).
22. S. Piazolo, A. La Fontaine, P. Trimby, S. Harley, L. Yang, R. Armstrong, J. M. Cairney, Deformation-induced trace element redistribution in zircon revealed using atom probe tomography. *Nat. Commun.* **7**, 10490 (2016).
23. T. Geisler, U. Schaltegger, F. Tomaschek, Re-equilibration of zircon in aqueous fluids and melts. *Elements* **3**, 43–50 (2007).
24. A. J. Cavosie, S. A. Wilde, D. Liu, P. W. Weiblen, J. W. Valley, Internal zoning and U-Th-Pb chemistry of Jack Hills detrital zircons: A mineral record of early Archean to Mesoproterozoic (4348-1576 Ma) magmatism. *Precambrian Res.* **135**, 251–279 (2004).
25. X. Quidelleur, M. Grove, O. M. Lovera, T. M. Harrison, A. Yin, F. J. Ryerson, Thermal evolution and slip history of the Renbu Zedong thrust, southeastern Tibet. *J. Geophys. Res.* **102**, 2659–2679 (1997).
26. C. Patterson, D. Settle, B. Glover, Analysis of lead in polluted coastal seawater. *Mar. Chem.* **4**, 305–319 (1976).
27. C. J. Spencer, C. L. Kirkland, R. J. M. Taylor, Strategies towards statistically robust interpretations of in situ U-Pb zircon geochronology. *Geosci. Front.* **7**, 581–589 (2016).
28. Q. Wang, S. A. Wilde, New constraints on the Hadean to Proterozoic history of the Jack Hills belt, Western Australia. *Gondw. Res.* **55**, 74–91 (2018).
29. E. A. Bell, P. Boehnke, M. D. Hopkins-Wielicki, T. M. Harrison, Distinguishing primary and secondary inclusion assemblages in Jack Hills zircons. *Lithos* **234–235**, 15–26 (2015).
30. M.-C. Liu, K. D. McKeegan, T. M. Harrison, G. Jarzebinski, L. Vltava, The Hyperion-II radio-frequency oxygen ion source on the UCLA *ims*1290 ion microprobe: Beam characterization and applications in geochemistry and cosmochemistry. *Int. J. Mass Spectrom.* **424**, 1–9 (2018).
31. E. A. Bell, T. M. Harrison, M. T. McCulloch, E. D. Young, Early Archean crustal evolution of the Jack Hills zircon source terrane inferred from Lu-Hf, $^{207}Pb/^{206}Pb$, and $\delta^{18}O$ systematics of Jack Hills zircons. *Geochim. Cosmochim. Acta* **75**, 4816–4829 (2011).
32. T. Berndt, A. R. Muxworthy, K. Fabian, Does size matter? Statistical limits of paleomagnetic field reconstruction from small rock specimens. *J. Geophys. Res. Solid Earth* **121**, 15–26 (2016).
33. G. A. Paterson, L. Tauxe, A. J. Biggin, R. Shaar, L. C. Jonestrask, On improving the selection of Thellier-type paleointensity data. *Geochem. Geophys. Geosyst.* **15**, 1180–1192 (2014).
34. P. W. Reiners, R. W. Carlson, P. R. Renne, K. M. Cooper, D. E. Granger, N. M. McLean, B. Schoene, *Geochronology and Thermochronology* (Wiley, 2017).

Acknowledgments: We acknowledge R. L. Walsworth for developing the QDM and T. F. Peterson Jr. for support. **Funding:** This study was supported by the NSF (grants EAR 1647504, EAR 1847042, and DMS 1521765) and the European Research Council under the European Union's Seventh Framework Programme (Grant FP/2007-2013)/European Research Council Grant Agreement 320750, Natural Environment Research

Downloaded from http://advances.sciencemag.org/ on April 9, 2020

Council Grant NE/P002498/1. The UCLA ion microprobe facility is partly supported by a grant from the Instrumentation and Facilities Program, Division of Earth Sciences, NSF (1339051). **Author contributions:** C.S.B. conducted paleomagnetic measurements, analyzed the data, and prepared the manuscript. B.P.W. conceived the project and carried out the advising. E.A.L. provided support on data analysis. F.T., R.J.M.T., J.F.E., and R.J.H. conducted measurements. R.R.F. conducted QDM measurements. E.A.B., E.W.A., H.M.K., M.M.W., and T.M.H. conducted microprobe measurements. J.R. separated the samples and provided support with acid washing. A.C.M. provided help with the manuscript preparation. **Competing interests:** The authors declare that they have no competing interests. **Data and materials availability:** All data needed to evaluate the conclusions in the paper are present in the paper and/or the Supplementary Materials. Additional data related to this paper may be requested from the authors.

Submitted 5 November 2018
Accepted 19 December 2019
Published 8 April 2020
10.1126/sciadv.aav9634

Citation: C. S. Borlina, B. P. Weiss, E. A. Lima, F. Tang, R. J. M. Taylor, J. F. Einsle, R. J. Harrison, R. R. Fu, E. A. Bell, E. W. Alexander, H. M. Kirkpatrick, M. M. Wielicki, T. M. Harrison, J. Ramezani, A. C. Maloof, Reevaluating the evidence for a Hadean-Eoarchean dynamo. *Sci. Adv.* **6**, eaav9634 (2020).

Downloaded from http://advances.sciencemag.org/ on April 9, 2020

Science Advances

Reevaluating the evidence for a Hadean-Eoarchean dynamo

Cauê S. Borlina, Benjamin P. Weiss, Eduardo A. Lima, Fengzai Tang, Richard J. M. Taylor, Joshua F. Einsle, Richard J. Harrison, Roger R. Fu, Elizabeth A. Bell, Ellen W. Alexander, Heather M. Kirkpatrick, Matthew M. Wielicki, T. Mark Harrison, Jahandar Ramezani and Adam C. Maloof

Sci Adv **6** (15), eaav9634.
DOI: 10.1126/sciadv.aav9634

ARTICLE TOOLS http://advances.sciencemag.org/content/6/15/eaav9634

SUPPLEMENTARY MATERIALS http://advances.sciencemag.org/content/suppl/2020/04/06/6.15.eaav9634.DC1

REFERENCES This article cites 33 articles, 3 of which you can access for free
http://advances.sciencemag.org/content/6/15/eaav9634#BIBL

PERMISSIONS http://www.sciencemag.org/help/reprints-and-permissions

Use of this article is subject to the Terms of Service

Science Advances (ISSN 2375-2548) is published by the American Association for the Advancement of Science, 1200 New York Avenue NW, Washington, DC 20005. The title *Science Advances* is a registered trademark of AAAS.

Copyright © 2020 The Authors, some rights reserved; exclusive licensee American Association for the Advancement of Science. No claim to original U.S. Government Works. Distributed under a Creative Commons Attribution NonCommercial License 4.0 (CC BY-NC).

Downloaded from http://advances.sciencemag.org/ on April 9, 2020